The object of this study is the measurement errors of a fiber-optic gyroscope, which is an element of the spacecraft orientation control system. The task to determine the patterns of thermomechanical loading influence on the measurement errors of gyroscopes has been solved by using mathematical modeling. The study was conducted using the finite element method, which has made it possible to analyze the stress-strain state of structural elements under different conditions of temperature and mechanical loading. Temperature and deformation distributions of the spacecraft structural elements were obtained. These data were used to estimate the misalignment parameters of the sensitivity axes of the onboard system gyroscopes, which arise due to structural deformation. Under certain modeling conditions, they exceed one hundred arc seconds, which could lead to an unacceptable error in controlling the spacecraft orientation.

To specify the magnitude of gyroscopes' measurement error, high-frequency oscillations that occur when the jet engine is turned on during the correction of the spacecraft's orbit were considered together with thermal deformation of the structure. This combination of thermal and mechanical effects creates conditions under which the accuracy of the control systems is significantly compromised. It was determined that under the conditions studied, the measurement error increases 8 times when the temperature of the structure changes by 40 °C.

Thus, to solve the task set, a procedure for determining the measurement error under specific conditions of thermomechanical loading was devised and described. Using such a procedure in the design of control systems in the future will contribute to increasing the accuracy of their operation. This will be achieved by optimally placing gyroscopes on board, taking into account the influence of thermal fields

Keywords: thermomechanical deformation, finite element method, misalignment of a fiber-optic gyroscope, measurement errors

UDC 539.3

DOI: 10.15587/1729-4061.2025.324960

DETERMINING THE INFLUENCE OF THERMOMECHANICAL LOADING ON THE MEASUREMENT ERRORS OF FIBER-OPTIC GYROSCOPE

Dmytro Breslavsky
Doctor of Technical Sciences, Professor*
Valerii Uspenskyi
Doctor of Technical Sciences, Professor*
Volodymyr Mietielov
Corresponding author
PhD, Associate Professor*
E-mail: volodymyr.mietielov@khpi.edu.ua
Alyona Senko
Doctor of Philosophy*
Oksana Tatarinova
PhD, Associate Professor*
*Department of Computer Modeling of Processes and Systems
National Technical University «Kharkiv Polytechnic Institute»
Kyrpychova str., 2, Kharkiv, Ukraine, 61002

Received 06.01.2025
Received in revised form 26.02.2025
Accepted 13.03.2025
Published

How to Cite: *Breslavsky, D., Uspenskyi, V., Mietielov, V., Senko, A., Tatarinova, O. (2025). Determining the influence of thermomechanical loading on the measurement errors of fiber-optic gyroscope. Eastern-European Journal of Enterprise Technologies, 2 (7 (134)), 50–65. https://doi.org/10.15587/1729-4061.2025.324960*

1. Introduction

During motion, spacecraft (SC) are exposed to the influence of inhomogeneous thermal fields, which lead to significant temperature strains of the structure and elements of SC. On the other hand, as a result of fuel combustion in the liquid propellant jet engine (LJE) of a rocket or spacecraft, cyclic loads occur. Such loads lead to oscillations of structural elements with a small amplitude, but with a high frequency. The impact of both of these factors on the operation of devices located on board aircraft could be critical. First, there may be a deterioration in the accuracy of SC orientation due to an increase in the errors of gyroscopic onboard systems. Second, there may be a loss of functionality because of the possible failure of on-board systems.

Analysis of the performance of rocket and space technology instruments located on board aircraft can be carried out in two ways. The first is purely experimental, in which conditions similar to operational ones are created at laboratory facilities. This technique is expensive, but most importantly, it makes it possible to obtain recommendations only for the tested device under the specified operating conditions. When upgrading an instrument or changing the operating characteristics, for example, when moving to another orbit, all conclusions and recommendations become irrelevant and there is a need to conduct new series of experiments.

The second technique is based on mathematical modeling of typical operating conditions of aircraft instruments, taking into account the characteristics of its motion. This technique, because of the complexity of its theoretical description and the development of methods and algorithms for mathematical modeling, is only beginning to evolve. Therefore, it is a relevant task to carry out studies on determining the influence of thermomechanical loads on gyroscope measurement errors based on mathematical modeling under specific operating conditions.

2. Literature review and problem statement

The operation of any spacecraft is accompanied by its certain spatial orientation. Such orientation is carried out by the

onboard control system, which, first of all, solves the task to determine the current orientation of the spacecraft. The accuracy of determining the orientation depends on the technique by which this is done and the errors of the measuring sensors. In [1], a technique for processing solar radiation measurements by sensors mounted on different surfaces of the spacecraft structure was devised and substantiated. The advantage of this technique is simplicity and reliability, but the main disadvantage is that it does not work in the shadow of the Earth. This approach is generalized in [2], in which, along with solar sensors, Earth magnetic field meters and a satellite radio navigation system signal receiver were used to determine the spacecraft orientation, which provides determination of the spacecraft coordinates for using the field model. Such a system will already work under any lighting conditions, but its accuracy significantly depends on the accuracy of the Earth's magnetic field model and the satellite's orbit altitude. In addition, the above sensors have a narrow bandwidth, which makes their effective use under conditions of high-frequency object oscillations impossible.

Another approach to determining orientation is more traditional and is based on the use of inertial sensors – gyroscopes. In [3], information on the use of inertial technologies in spacecraft orientation control systems is presented and systematized. A comparison of modern gyroscopes, including fiber-optic gyroscopes (FOGs), is given in terms of their accuracy. The main way to increase the accuracy of gyroscopic measurements is determined by designing gyroscopes based on new physical principles. It is worth noting that the authors does not pay enough attention to the sensitivity of gyroscope measurement errors to temperature factors and the possibilities of reducing it through calibration and compensation.

Analysis and compensation of the temperature dependence of FOG errors are given in [4], in which an improved method of taking into account the FOG temperature and filtering its measurements when determining the actual drift is proposed. The improved method makes it possible to compensate for the temperature-dependent drift with high accuracy. On the other hand, the significant dependence of FOG error on the temperature gradient can be reduced by the hardware measures proposed in [5]. But it is impossible to limit ourselves to those two studies to solve the problem of compensating for FOG measurement errors because they do not take into account the errors that arise due to the misalignment of FOG relative to the nominal position of its sensitivity axis. For such consideration, it is necessary to analyze FOG as part of a specific design of the orientation system. Certain results in this direction are reported in [6], in which an experimental method for calibrating the parameters of FOG misalignment of the inertial system is proposed. But the issue of determining the error in FOG measurements due to misalignment depending on the temperature of the structure on which the gyroscope is located remains unresolved.

As shown in [7], during a flight in low orbit, the displacement of normals to different faces of a cubic satellite due to non-stationary heating by solar rays can reach 100″. This means that the structural elements to which the FOG is attached may also have certain deformation that will cause the FOG misalignment. A misalignment of 5″ may be critical from the point of view of the accuracy of determining the orientation of the spacecraft. Therefore, it is important to determine the possible temperature effect on FOG readings at the design stage of the on-board layout with the aim of its subsequent compensation.

Experimental methods for solving this problem require special equipment and are not very appropriate because the task must be solved at the design stage. On the other hand, real objects of analysis have a rather complex geometric shape, and their operation is characterized by initial and boundary conditions with complex geometry. Therefore, it is difficult to apply well-developed and tested exact analytical methods [8] to analysis in most cases. In this regard, numerical methods are used to solve applied problems of mechanics and stationary and non-stationary thermal conductivity, among which the finite element method (FEM) takes the first place [9].

The most common is the case of non-stationary thermal conductivity, when, as a result of changes in temperatures, heat flows, and other factors, the temperature in the object of study constantly changes in time. The conclusions reported in [8, 9] show that, if there are data on the boundary conditions describing the motion of the satellite in the near-Earth orbit, the use of FEM provides quite satisfactory calculated data on the temperature distribution. FEM application is also effective in the analysis of thermal strength and vibration processes [9].

Thus, the general problem of achieving high accuracy of spacecraft orientation control, taking into account world experience, is expedient to solve by using FOGs because they are quite accurate and resistant to vibration. For them, the issue of the influence of thermal fields and temperature error models has already been considered earlier [10]. At the same time, the influence of thermomechanical loads that occur during the flight of the spacecraft, namely on the misalignment of FOG, has not yet been studied. Therefore, when addressing the task set, it is considered advisable to focus on determining the measurement error caused by FOG misalignment, which occurs under the influence of typical thermomechanical loads. The principal method for the determination procedure is FEM.

3. The aim and objectives of the study

The purpose of our study is to determine the influence of thermal fields and vibration loads on the measurement errors of a fiber-optic gyroscope, which is part of the spacecraft (SC) orientation control system, based on mathematical modeling. Such a study, conducted for specific conditions of thermomechanical loads, will provide an opportunity to increase the accuracy of the spacecraft control system by optimizing the location of on-board equipment.

To achieve the goal, the following tasks were set:

– to model the operating conditions of FOG and to calculate the thermomechanical deformation of structural elements in which the fiber-optic gyroscopes of the onboard orientation system can be located;

– to calculate and analyze the measurement errors of the fiber-optic gyroscope at certain thermomechanical deformation.

4. The study materials and methods

The object of our study is the measurement errors of a fiber-optic gyroscope due to thermomechanical loads that occur during the operation of spacecraft.

The following hypothesis of the study has been put forward. Thermal fields on board the spacecraft lead to deformation of structural elements. Such deformation due to unequal displacements of the points of attachment of FOG

to the spacecraft body leads to misalignment of the actual axis of sensitivity of the gyroscope with the calculated ideal direction. Under dynamic conditions, such misalignment causes measurement errors that could lead to a decrease in control accuracy.

To verify the stated hypothesis, methods of continuum mechanics are used, in particular thermoelasticity, solid body dynamics, and metrology.

The general mathematical statement of the boundary value problem of deformation of bodies of volume V with isotropic material properties implies the Cartesian coordinate system x_i (i=1, 2, 3). Volumetric forces, with the exception of inertia forces, are considered absent. The body can be uniformly or non-uniformly heated, i.e. be in a non-uniform temperature field $T=T(x_i,t)$. Boundary conditions: on a part of the body surface S_1, time-invariant, corresponding to the fixation, displacements $u_{i|S_1}=\overline{u}_i$ are given. On another part of the body surface S_2, surface forces $p(x)$ are applied, which can have a static p_0 and a cyclically varying component with amplitude:

$$p=p_0+p_a\sin 2\pi\omega t. \tag{1}$$

Here, for certainty, the process of harmonic oscillations with frequency ω is considered.

According to the Lagrangian description of the kinematics of an arbitrary point of the body, small strains and displacements are considered. The following notations are used: **u** – displacement vector with components $u_i(x_i,t)$; **σ, ε** – stress and strain tensors with components $\sigma_{ij}=\sigma_{ji}(x_i,t)$ and $\varepsilon_{ij}=\varepsilon_{ji}(x_i,t)$, which are functions of the coordinates of the point of the body x_i (i=1, 2, 3) and time t. The statement involves using the classical hypothesis on the additivity of stains: at any time, the complete strain tensor is the sum of the elastic and temperature strain tensors:

$$\varepsilon_{ij}=\boldsymbol{\varepsilon}_{ij}^{el}+\boldsymbol{\varepsilon}_{ij}^{T}, \tag{2}$$

where $\boldsymbol{\varepsilon}^{el}$, $\boldsymbol{\varepsilon}^{T}$ are the elastic and temperature strain tensors, respectively.

For thermoelastic strains, the generalized law of thermoelasticity of homogeneous isotropic bodies is used in the form known as the Duhamel-Neumann law [11, 12]. At any time, the relationship between stresses and strains and temperature can be written as:

$$\sigma_{ij}=\lambda\varepsilon_0\delta_{ij}+2G\varepsilon_{ij}-(3\lambda+2G)\varepsilon_{ij}^{T}, \tag{3}$$

$$\varepsilon_0=\varepsilon_{km}\delta_{km},\ \lambda=\frac{\nu E}{(1+\nu)(1-2\nu)},\ G=\frac{E}{2(1+\nu)},\ \varepsilon_{ij}^{T}=\alpha T\delta_{ij},$$

where λ, G are the Lamé parameters of the elastic properties of the material; E and ν are the elastic modulus and Poisson's ratio of the material; α, δ_{ij} are the thermal expansion coefficient and Kronecker delta; i, j, k, m =1, 2, 3.

The volumetric strain corresponds to thermoelastic compressibility [11]:

$$\varepsilon_0=\varepsilon_{ij}\delta_{ij}=\varepsilon_{11}^{el}+\varepsilon_{22}^{el}+\varepsilon_{33}^{el}+3\alpha T. \tag{4}$$

The basic system of equations for determining the thermoelastic stress-strain state of a body under conditions of a known temperature field is represented as follows [11–13]:

$$\begin{aligned}
&\sigma_{ij,j}=\rho u_{tt},\ \sigma_{ij}n_j=p_i(x),\ x_i\in S_2;\\
&\varepsilon_{ij}=\frac{1}{2}(u_{i,j}+u_{j,i}),\ x_i\in V;\ u_i\big|_{S_1}=\overline{u}_i,\ x_i\in S_1;\\
&\sigma_{ij}=\lambda\varepsilon_0\delta_{ij}+2G\varepsilon_{ij}-(3\lambda+2G)\alpha T\delta_{ij},
\end{aligned} \tag{5}$$

where, in addition to the previously defined notations, n is the unit vector of the external normal to surface S_2 of the body with components n_i, i=1, 2, 3.

To determine the time-varying temperature field of a structural element or device, for example, when a spaceship is moving in a near-Earth orbit, the problem of non-stationary heat conduction is solved [14]:

$$\begin{aligned}
\rho(T)c_T(T)\cdot\frac{\partial T}{\partial t}&=\frac{\partial}{\partial x_1}\left(\lambda_T(T)\frac{\partial T}{\partial x_1}\right)+\\
&+\frac{\partial}{\partial x_2}\left(\lambda_T(T)\frac{\partial T}{\partial x_2}\right)+\frac{\partial}{\partial x_3}\left(\lambda_T(T)\frac{\partial T}{\partial x_3}\right)+Q_T(x_i,t),
\end{aligned} \tag{6}$$

where λ_T – thermal conductivity coefficient; c_T, ρ – distributed heat capacity and density of the material, respectively; $Q_T(x_i,T)$ – generalized volumetric thermodynamic forces.

Additional conditions to equation (6) consist of the initial ones:

$$T(x_i,0)=\hat{\psi}(x_i),\ i=1,2,3, \tag{7}$$

and boundary conditions that can be specified on different parts (S_3–S_6) of surface S. The main boundary conditions that can be added to equation (6): given temperature varying over time (Dirichlet condition) – surface S_3; given heat flux (Neumann condition) – surface S_4; heat transfer by convective heat exchange (Newton-Richmann condition) – surface S_5; heat transfer by radiative heat exchange (Stefan-Boltzmann condition) – surface S_6 [14]:

$$\begin{aligned}
&T\big|s_3=\theta(t),\\
&\frac{\partial T}{\partial n}\big|s_4=q(t),\\
&\frac{\partial T}{\partial n}\big|s_5=\alpha_{Conv}\cdot(T_{Env}-T),\\
&\frac{\partial T}{\partial n}\big|s_6=\varepsilon_{Black}\cdot\delta_{SB}\cdot(T_{Env}^4-T^4),
\end{aligned} \tag{8}$$

where $\theta(t)$ is a given function of temperature varying over time; $q(t)$ is a given heat flux; $\alpha_{Conv}=\alpha_{Conv}(T)$ is the heat transfer coefficient, $\frac{\mathrm{W}}{\mathrm{m}^2\times^\circ\mathrm{C}}$; T_{Env} is the ambient temperature; $\varepsilon_{Black}=\varepsilon_{Black}(T)$ is the blackness coefficient; $\delta_{SB}=5.670367\cdot10^{-8}$ is the Stefan-Boltzmann constant, $\frac{\mathrm{W}}{\mathrm{m}^2\times^\circ\mathrm{C}^4}$.

The found values of temperatures at each point of the body at any time $T=T(x_i,t)$ are used to determine the components of volumetric thermoelastic deformation. Also, knowledge of temperature changes is necessary for accurate consideration of the physical and mechanical properties of the material, which significantly depend on it.

Today, there is practically no alternative for the finite element method (FEM, [15]) to be used in the analysis of structural elements with real geometry and real boundary conditions. To apply it for solving formulated elasticity problems in the presence of vibration or thermal loads (5) and non-stationary thermal conductivity (6), a transition to variational statement of the problems is performed.

Solving both problems (5) and (6) occurs together. Given the given boundary and initial conditions, the solution to the system of equations (6) determines the temperature field acting on the structural element, and then, taking it into account, the necessary elastic problems of type (5) are solved. Displacements and strains in the required areas of the equipment are determined, which are subsequently taken into account when determining the errors of instruments. To solve the problems, the ANSYS software [16] (country of origin USA) is used, which is intended, among other things, for conducting professional engineering calculations in the field of thermomechanics. A volumetric finite element in the form of a parallelepiped is used.

5. Results of determining and investigating the measurement error of a fiber-optic gyroscope under the influence of thermomechanical loads

5. 1. Determining the deformed state of rocket and space technology elements due to temperature and vibration loads

At the first stage of the study, an estimate of the stress-strain state of the two-stage rocket model when the engine is turned on was obtained. Numerical modeling of the stress-strain state was carried out for the calculation scheme of the two-stage rocket model with a liquid propellant jet engine (LJE), the main geometric dimensions of which are shown in Fig. 1.

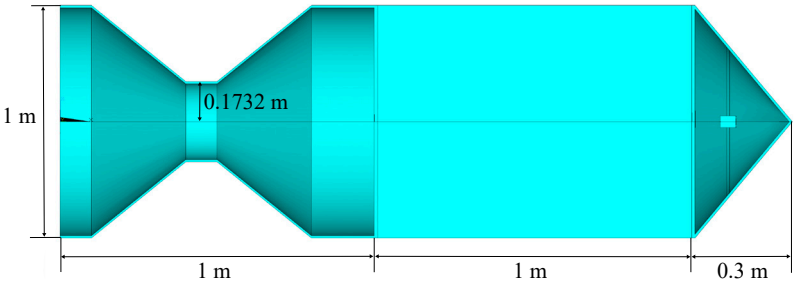

Fig. 1. Calculation diagram of a two-stage rocket

The launch moment of a vertically mounted rocket with the LJE turned on has been analyzed. It is assumed that the first stage of the rocket, which is essentially the LJE, is made of heat-resistant alloy of type EI867 [17]. In the calculations, we used the physical and mechanical properties of the specified material at T=900 °C – elastic modulus, E=1.5·10^5 MPa; Poisson's ratio, ν=0.3; density, ρ=7.8·10^3 kg/m^3. It is assumed that the walls of the LJE chamber are uniformly heated to the specified temperature, and therefore temperature stresses are not taken into account.

The material of the second stage body is aluminum alloy of type D16AT with elastic modulus E=3.3·10^4 MPa, Poisson's ratio ν=0.3, density ρ=3.8·10^3 kg/m^3 [18]. At the moment of engine start-up, the body temperature is 20 °C. In the conical part of the compartment at a distance of 0.1 m from the cylindrical part, on cantilever holders 0.05 m long, symmetrically on both sides, there is a module of instruments in the form of a cube with a side of 0.05 m. The material properties of this model are taken as averaged – the modulus of elasticity and Poisson's ratio correspond to the material of the case (aluminum alloy of type D16AT), the density value is taken as ρ=2.5·10^3 kg/m^3.

When the engine is turned on, fuel pulsations begin on its inner surface [19], caused by the non-stationary combustion process. This process was modeled in the first approximation using relation (1), where p^0=2 MPa is the static pressure component, p^a=0.5 MPa is the amplitude pressure component, ω=1500 Hz is the vibration frequency.

The computational studies were performed using FEM. After building a finite element model of the object (symmetry conditions were applied), a numerical simulation of the thermoelasticity problem was performed and the distributions of stresses, strains, and displacements in the nodes and elements of the used meshes were determined. After convergence studies, a mesh of 50,000 finite elements was adopted.

The calculations were performed up to the moment of 1 s. Some results are shown in Fig. 2–7. Fig. 2, 3 depict the distributions of the total displacements along the rocket body at t=0.1 s and t=1 s. The displacements of the points of the instrument model were analyzed in more detail. For the analysis, four points on the surface of the instrument were involved, corresponding to the nodes of the FE model – three on one plane, and the other on a parallel one. They are marked with the letters A, B, C, D. The nature of the relative displacements of the nodes is similar, therefore, Fig. 5, 6 show the characteristics of two of them. Fig. 5, 6 depict the plots of varying in the values of the components of displacements u, v, and w depending on time for nodes D and A.

As an example, Fig. 7 shows the distributions of the Mises stress values over the volume of the rocket model body at t=1 s.

The next results of the study are to determine the deformed state of the instrument model during the motion of the artificial Earth satellite in a near-Earth orbit.

Numerical simulation of the deformation of a simplified instrument model was carried out under the condition of thermal conditions corresponding to the motion of the satellite in a near-Earth orbit for 3,600 s (1 hour). The model consists of two modules: an outer casing and a parallelepiped in the middle, which models the instrument module (Fig. 8).

The following values of mechanical and thermophysical properties of materials were used in our calculations. For the casing: Young's modulus E=35,000 MPa, Poisson's ratio ν=0.29, density ρ=2,000 kg/m^3, specific heat coefficient c_T=230 J/(kg·K), thermal conductivity coefficient λ_T=350 W/(m·K), linear expansion coefficient α=5 10^{-5} K^{-1}). For the internal module of instruments: Young's modulus E=35,000 MPa, Poisson's ratio ν=0.29, density ρ=2,000 kg/m^3, specific heat coefficient c_T=180 J/(kg·K), thermal conductivity coefficient λ_T=350 W/(m·K), linear expansion coefficient α=5·10^{-5} K^{-1}).

To perform calculations of the thermoelastic problem, SOLID226 and SURF152 finite elements were used. First, the non-stationary heat conduction problem was solved, and the temperature distribution was determined according to the model. On the side surface, boundary conditions of the 4th kind were set – Stefan-Boltzmann boundary conditions, which describe the processes of heat transfer by radiative heat exchange (blackness coefficient ε_{Black}=0.3, ambient temperature T_{env}=385 K).

In parallel, for this model with the specified nodal temperature values, the calculation of thermoelastic problems was carried out, the boundary conditions for which corresponded to fixing three points: 2 of them are corner, and one more on the opposite side in the middle of the side face. After conducting studies on the convergence of the results, a model of 15,952 finite elements and 30,250 nodes was adopted for calculations. The actual finite element model is shown in Fig. 9.

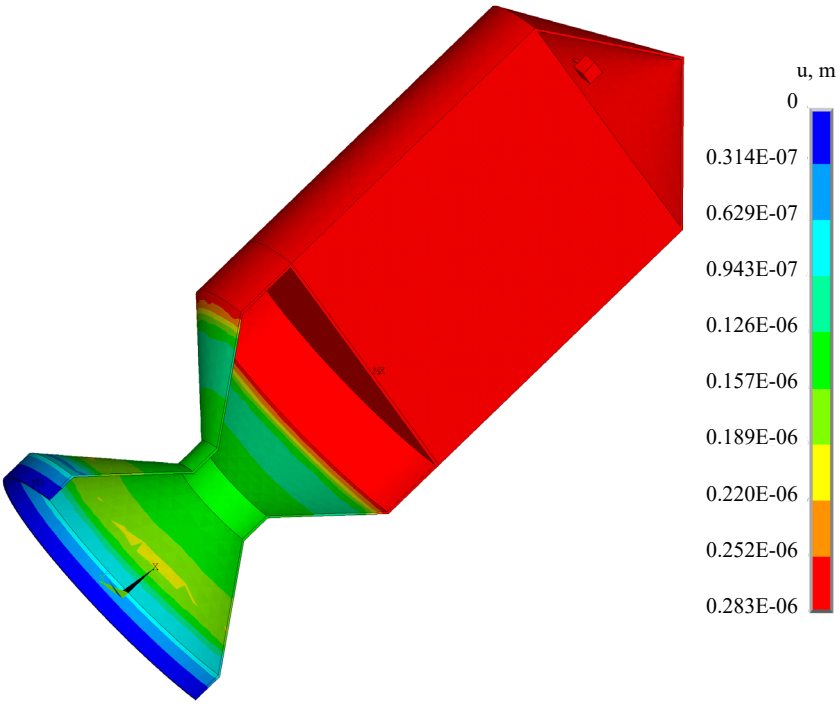

Fig. 2. Distribution of total displacements over the body, t=0.1 s

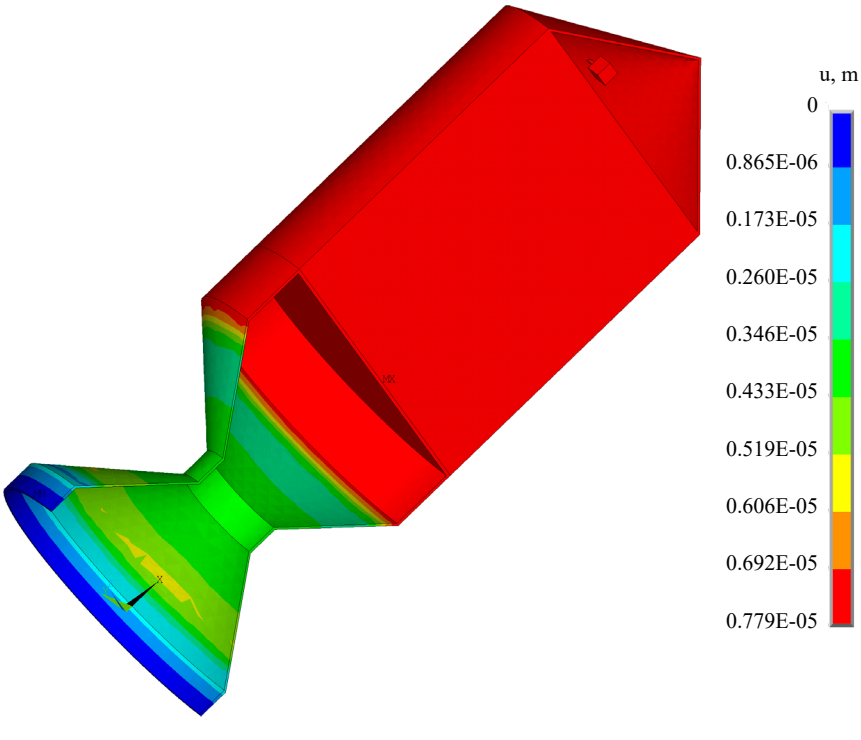

Fig. 3. Distribution of total displacements over the body, t=1 s

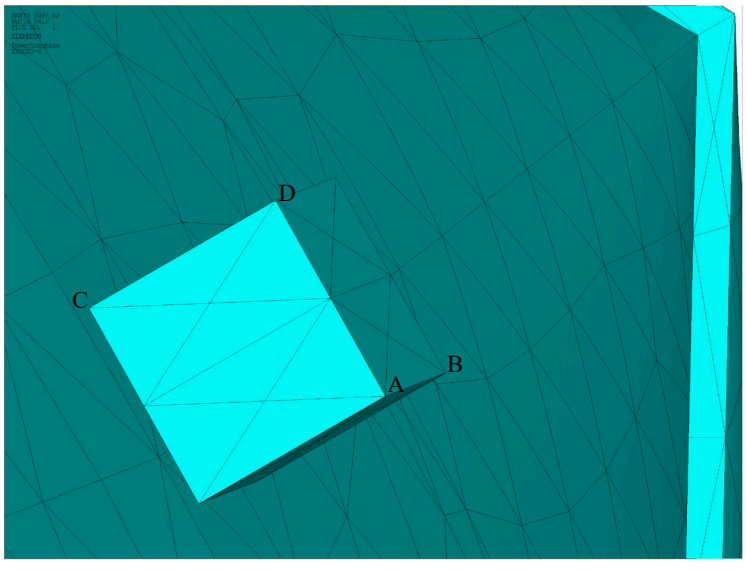

Fig. 4. Fragment of the FE mesh with the location of the model nodes in which the displacements are analyzed

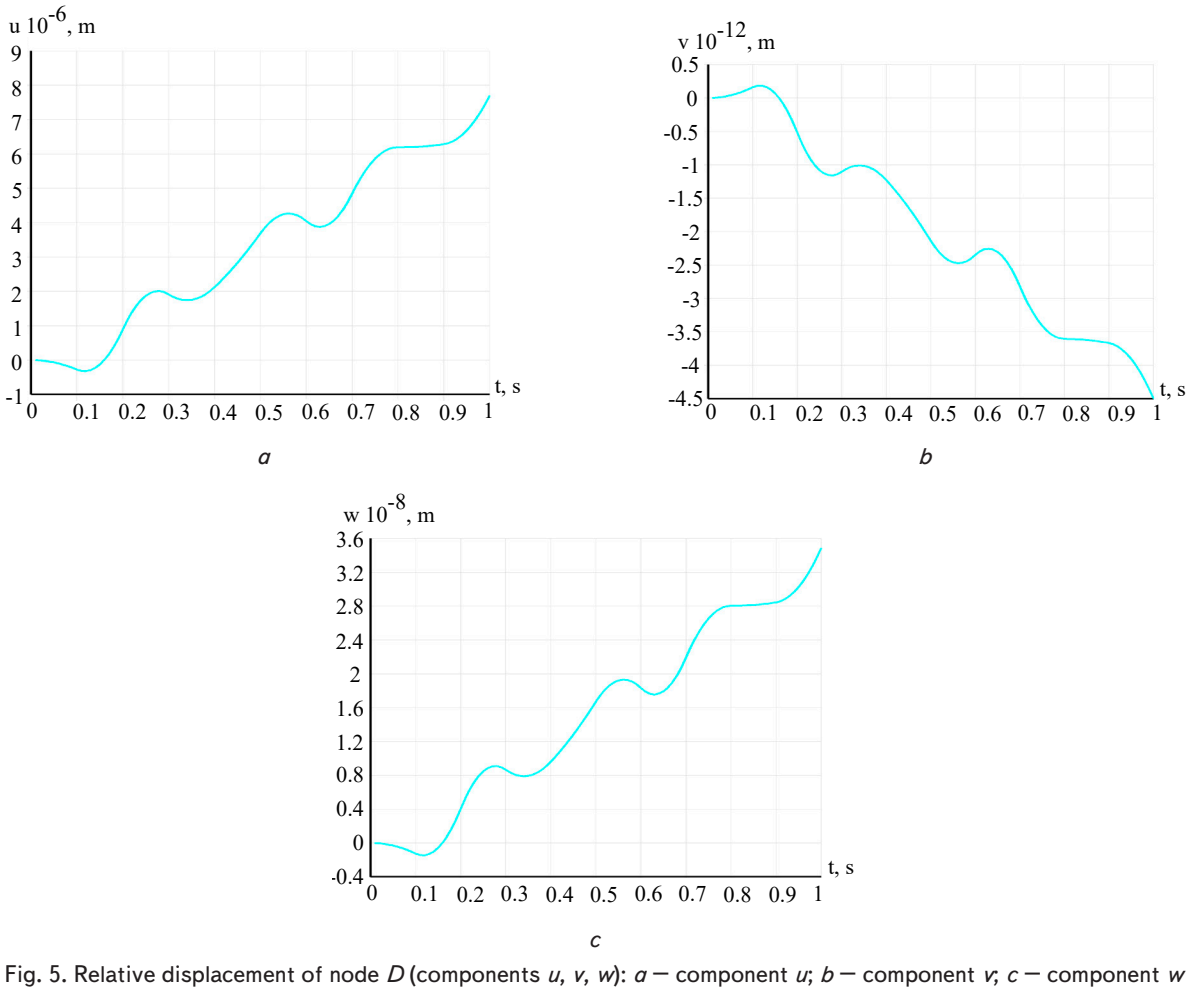

Fig. 5. Relative displacement of node *D* (components *u*, *v*, *w*): *a* — component *u*; *b* — component *v*; *c* — component *w*

The stress-strain state of the instrument model was simulated for all moments of the considered time of 3,600 s. As an example, Fig. 10, 11 show the distributions of the temperature and total displacements according to the model for two time points t=310.667 s and t=3,600 s.

The dependences of the components of the displacement vector on time have been constructed. They reflect the nature of deformation of the surface of an instrument module over time.

The designation of the points is shown in Fig. 12, which depicts a top view of the internal module of the model.

Fig. 13–15 show the resulting plots of the dependence of displacements on time at points *A*, *B*, *C* (Fig. 12).

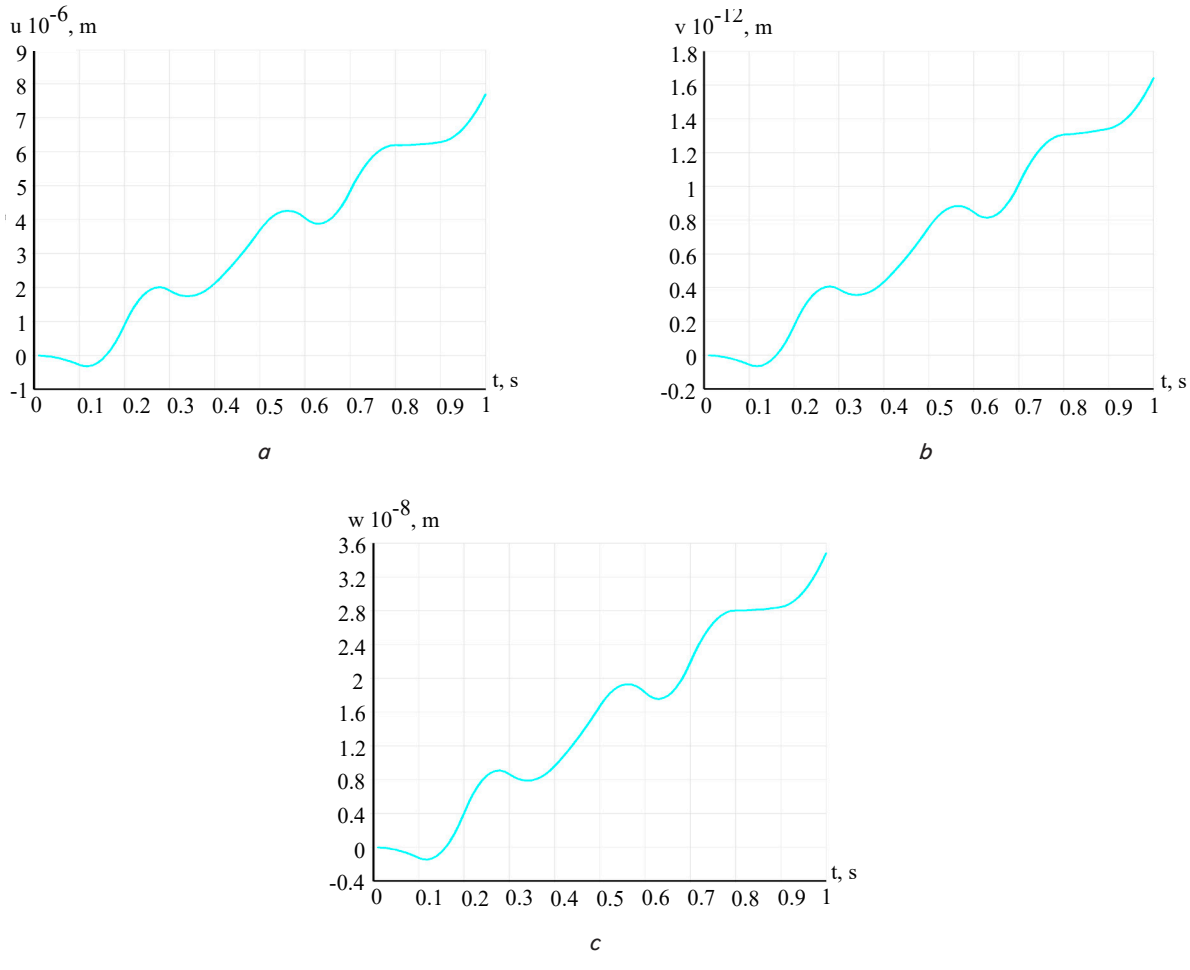

Fig. 6. Relative displacement of node *A* (components *u*, *v*, *w*): *a* – component *u*; *b* – component *v*; *c* – component *w*

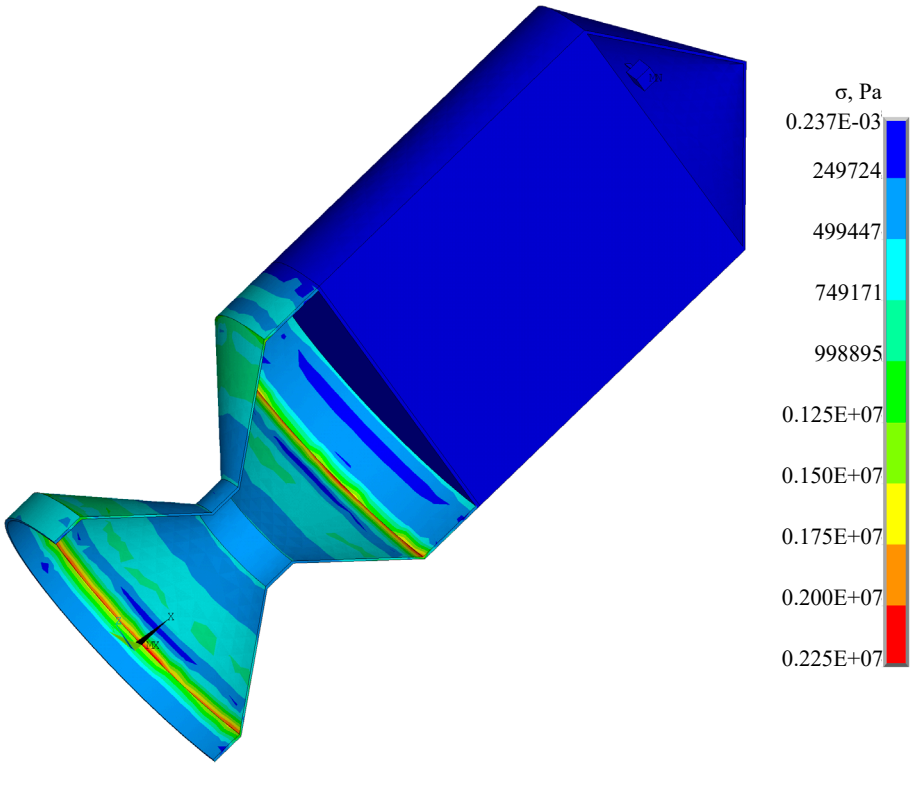

Fig. 7. Mises stress distribution, Pa, t=1 s

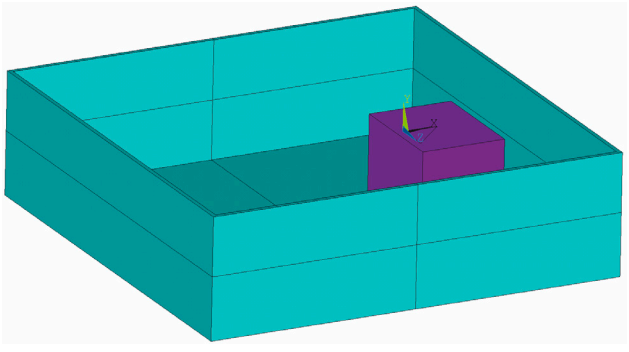

Fig. 8. Calculation model of the instrument module

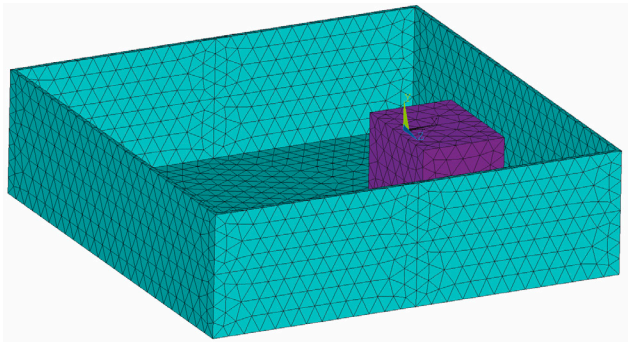

Fig. 9. Finite element model of the module

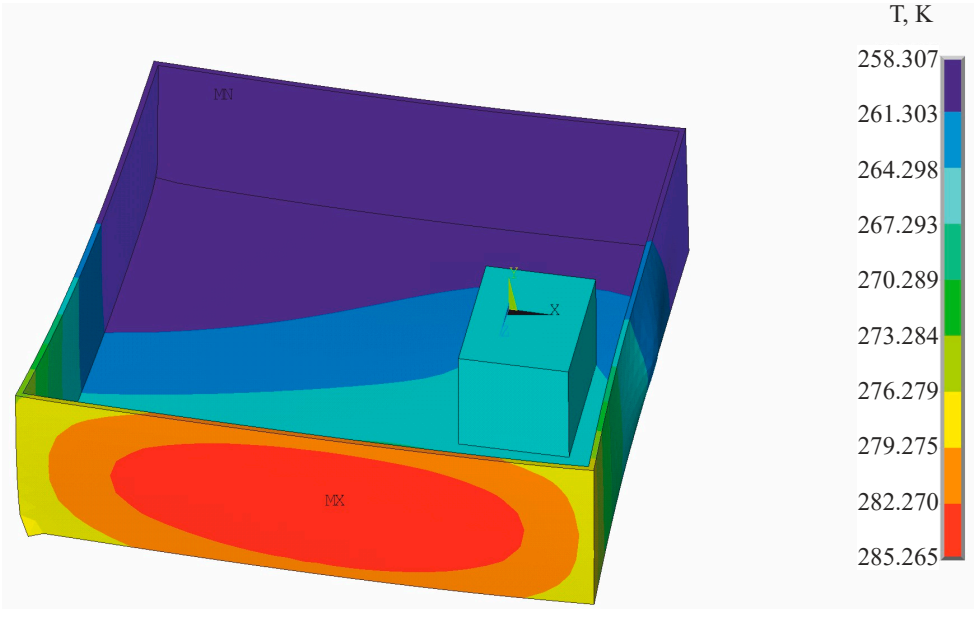

a

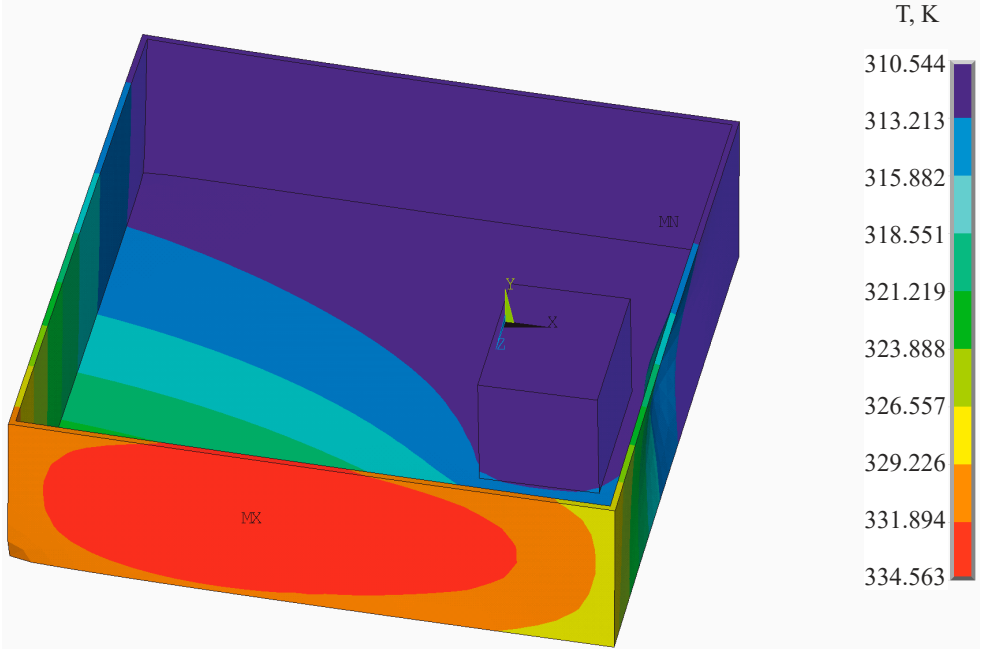

b

Fig. 10. Distribution of the temperature field over a module: *a* – *t*=310.667 s; *b* – *t*=3,600 s

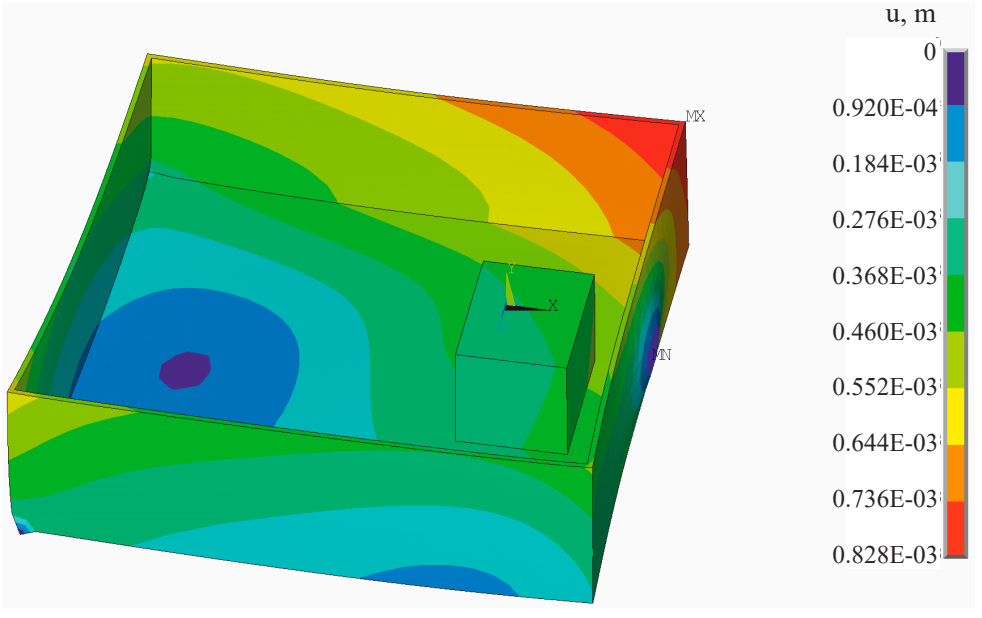

a

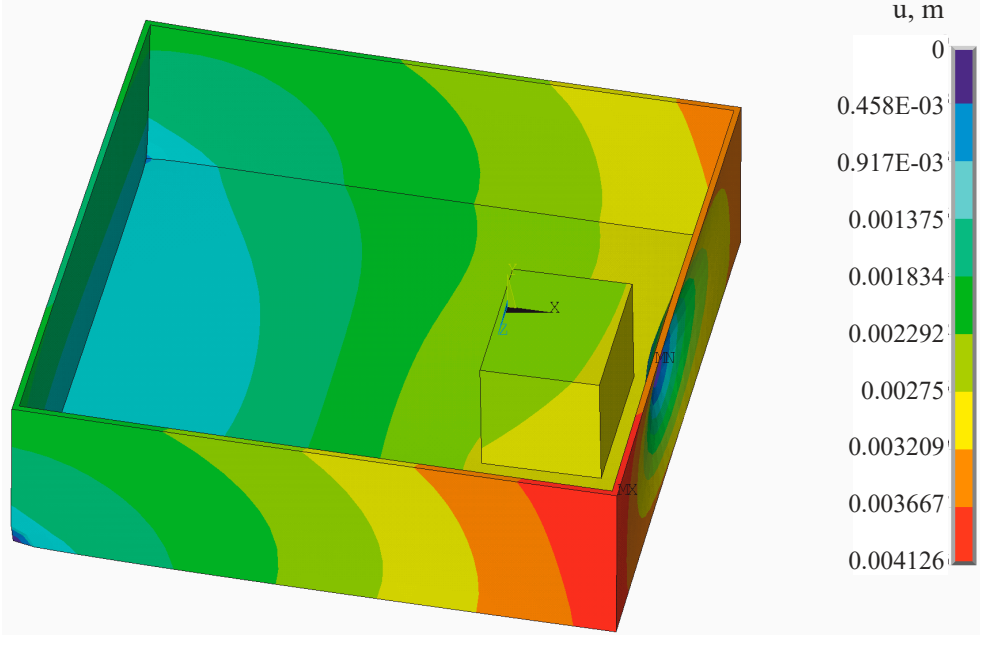

b

Fig. 11. Distribution of total displacements over a module: *a* – *t*=310.667 s; *b* – *t*=3,600 s

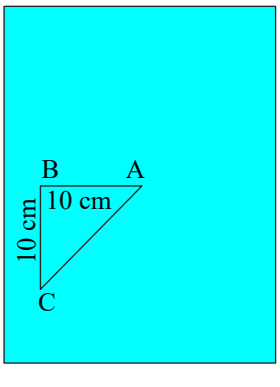

Fig. 12. Position of points for displaying the plots of dependence of the components of the displacement vector on time

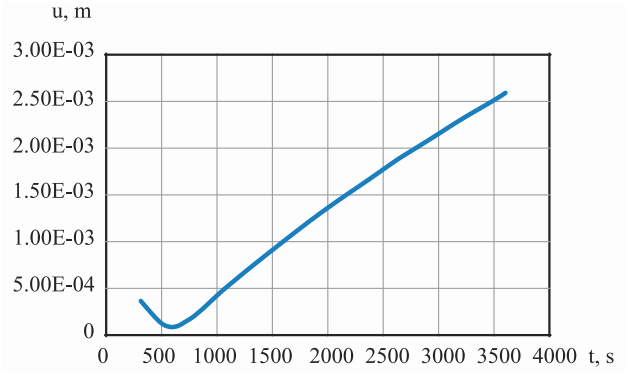

a

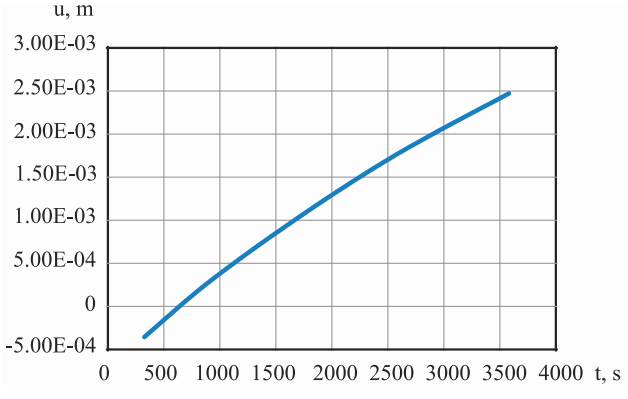

b

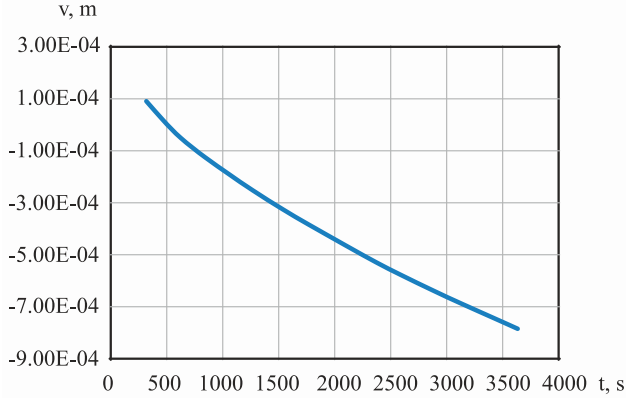

c

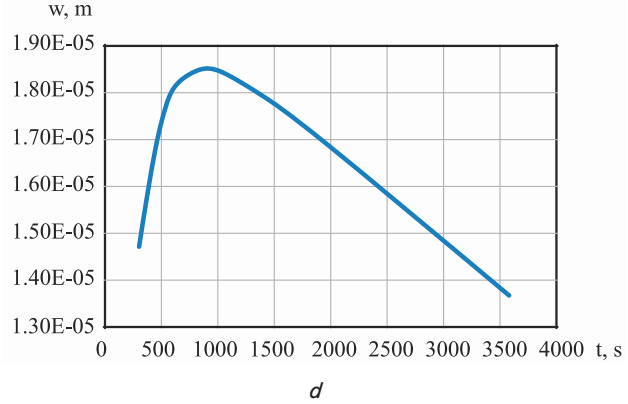

d

Fig. 13. Time dependence plots: *a* — total displacements; *b* — displacement component *u* (along the *X* axis); *c* — displacement component *v* (along the *Y* axis); *d* — displacement component *w* (along the *Z* axis) (point *A*)

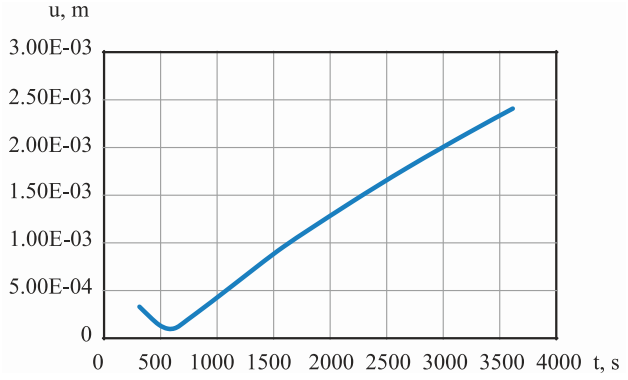

a

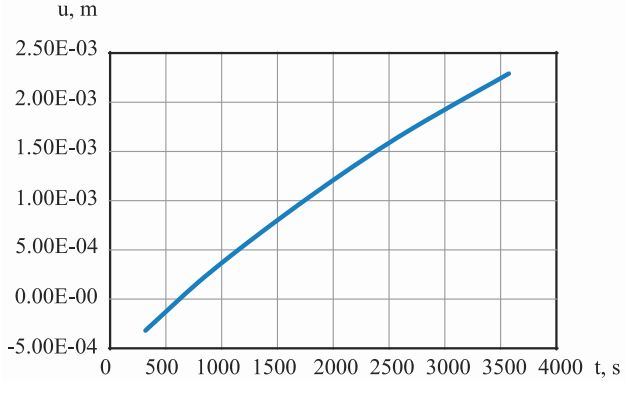

b

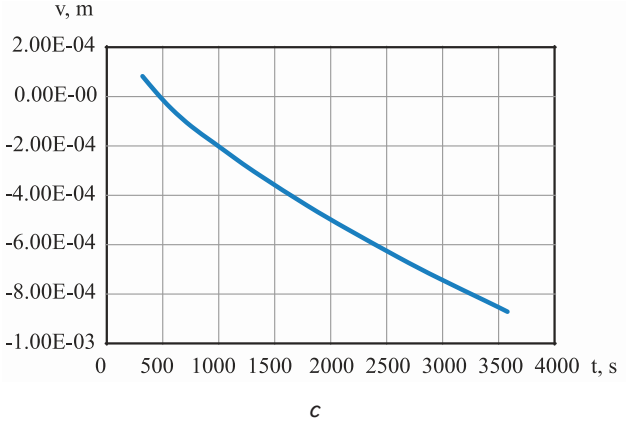

c

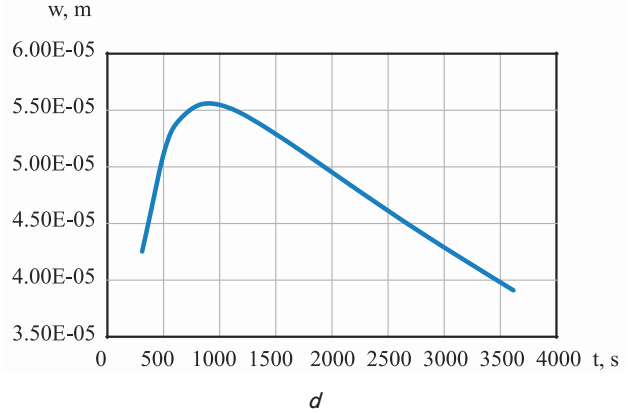

d

Fig. 14. Time dependence plots: *a* — total displacements; *b* — displacement component *u* (along the *X* axis); *c* — displacement component *v* (along the *Y* axis); *d* — displacement component *w* (along the *Z* axis) (point *B*)

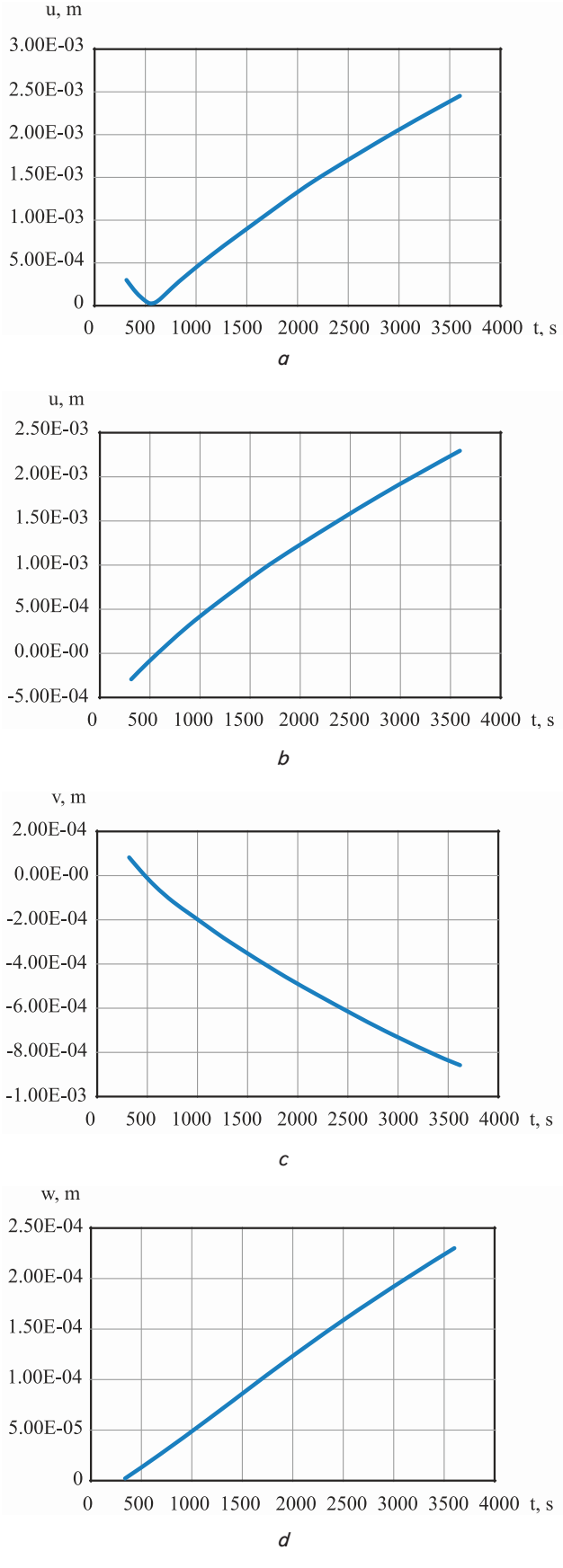

Fig. 15. Time dependence plots: *a* — total displacements; *b* — displacement component *u* (along the *X* axis); *c* — displacement component *v* (along the *Y* axis); *d* — displacement component *w* (along the *Z* axis) (point *C*)

5. 2. Determining errors of a fiber-optic gyroscope at specific thermomechanical deformation

Four points $O_{\{E\}}$, $X_{\{E\}}$, $Y_{\{E\}}$, $Z_{\{E\}}$ of a moving object were chosen in such a way that an orthogonal instrument coordinate system $\{E\}$ could be constructed on them, connected with the orientation determination system (Fig. 16). Fig. 16 shows an inertial coordinate system $\{I\}$, relative to which the position of points $O_{\{E\}}$, $X_{\{E\}}$, $Y_{\{E\}}$, $Z_{\{E\}}$ located on the object is given using radius vectors $\bar{R}_0$, $\bar{R}_1$, $\bar{R}_2$, $\bar{R}_3$. An orthogonal SC instrument coordinate system $\{E\}$ with the origin at point $O_{\{E\}}$ was constructed at these points. In addition to the radius vectors $\bar{R}_0$, $\bar{R}_1$, $\bar{R}_2$, $\bar{R}_3$, according to the calculation methodology, their derivatives $\bar{R}_0$, $\bar{R}_1$, $\bar{R}_2$, $\bar{R}_3$, or velocities $\bar{V}_0$, $\bar{V}_1$, $\bar{V}_2$, $\bar{V}_3$ are also known.

Under these conditions, the task is to determine the errors in FOG measurements as a result of the relative motion of the gyroscope attachment points to the body due to possible thermal deformation.

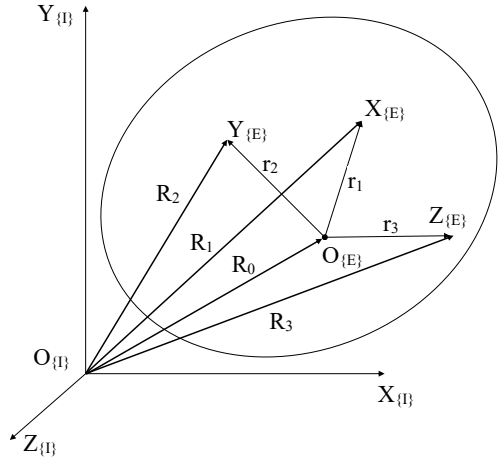

Fig. 16. Inertial and instrument coordinate systems, sensor placement points, and radius vectors of their positions

A gyroscope has been considered whose sensitivity axis is closest to the *i*-th axis of the instrument coordinate system ($i \in \{x,y,z\}$). The measurement error of the gyroscope is understood as follows. Among the components of error of the *i*-th gyroscope, which are physically localized separately, the drift $\delta\omega_i$, the scale factor error δk_i, and the misalignment parameters ρ_{ij}, ρ_{ik} of the sensitivity axes of FOG with the axes of the calculated instrument system are distinguished:

$$\Delta\omega_i(T,\Delta T) = \delta\omega_i(T,\Delta T) + \delta k_i(T)\cdot\omega_i + \\ +\rho_{ij}(T,\Delta T)\cdot\omega_j + \rho_{ik}(T,\Delta T)\cdot\omega_k, \quad (9)$$

where $(i, j, k)=(x, y, z)$ are indices subject to cyclic permutation; $\Delta\omega_i$ is the cumulative error of the *i*-th gyroscope; the dependence of the corresponding parameter on temperature T and the rate of its change ΔT is indicated in brackets.

Unlike drifts and the scale factor error, only the misalignment parameters are completely due to thermal deformation of the instrument structure. Their influence depends on the values of the current angular velocity of the spacecraft.

The calculation formulas for determining the angular velocity under vibration conditions on the data of point displacements in the general case were derived in [20].

The formulas for calculating the projections of the angular velocity ω_1, ω_2, ω_3 on the axis of the instrument coordinate system $X_{\{E\}}$, $Y_{\{E\}}$, $Z_{\{E\}}$ take the form:

$$\omega_1 = 0.5\frac{\left(\overline{r}_3, \Delta\overline{V}_2\right) - \left(\Delta\overline{V}_3, \overline{r}_2\right)}{\left\|\overline{r}_3\right\| \cdot \left\|\overline{r}_2\right\|},$$

$$\omega_2 = 0.5\frac{\left(\overline{r}_1, \Delta\overline{V}_3\right) - \left(\Delta\overline{V}_1, \overline{r}_3\right)}{\left\|\overline{r}_3\right\| \cdot \left\|\overline{r}_1\right\|},$$

$$\omega_3 = 0.5\frac{\left(\overline{r}_2, \Delta\overline{V}_1\right) - \left(\Delta\overline{V}_2, \overline{r}_1\right)}{\left\|\overline{r}_2\right\| \cdot \left\|\overline{r}_1\right\|}, \quad (10)$$

where $\overline{r}_i = \overline{R}_i - \overline{R}_0$, $\Delta\overline{V}_i = \overline{V}_i - \overline{V}_0$, $i = \overline{1,3}$.

To determine the angular velocity of a FOG module during engine start-up, the results of calculations of the deformed state of the instrument model were used, an example of which is shown in Fig. 4, 5. The effect of high-frequency vibrations on the instrument located in the front part of the object was studied.

A coordinate system (longitudinal X axis) is associated with this object, in which the base points modeling UCS are specified. Nodes and point coordinates (in m) are given in Table 1.

In the process of modeling, at a time interval of 2.5 ms, oscillations with a frequency of 1500 Hz, arising due to fuel combustion in the jet engine chamber, the displacement of all base points of the model of the instrument under consideration was obtained.

Table 1

Node numbers and point coordinates (in m)

Node	X	Y	Z	Comment
B	2.100	0.223	–0.025	sets the X axis of instrument CS
A	2.150	0.223	–0.025	origin of instrument CS
C	2.150	0.273	–0.025	sets the Z axis of instrument CS
D	2.150	0.223	0.025	sets the Y axis of instrument CS

Using formulas (10) for the base points, the following results were obtained. The estimate of the angular velocity takes the form shown in Fig. 17–19.

The small level of angular velocities is associated with the limited modeling conditions. With increasing intensity of dynamic influence, instantaneous angular velocities increase proportionally. The obtained values of angular velocity, characteristic of high-frequency oscillations, were used to determine the errors of gyroscope measurements due to misalignment parameters.

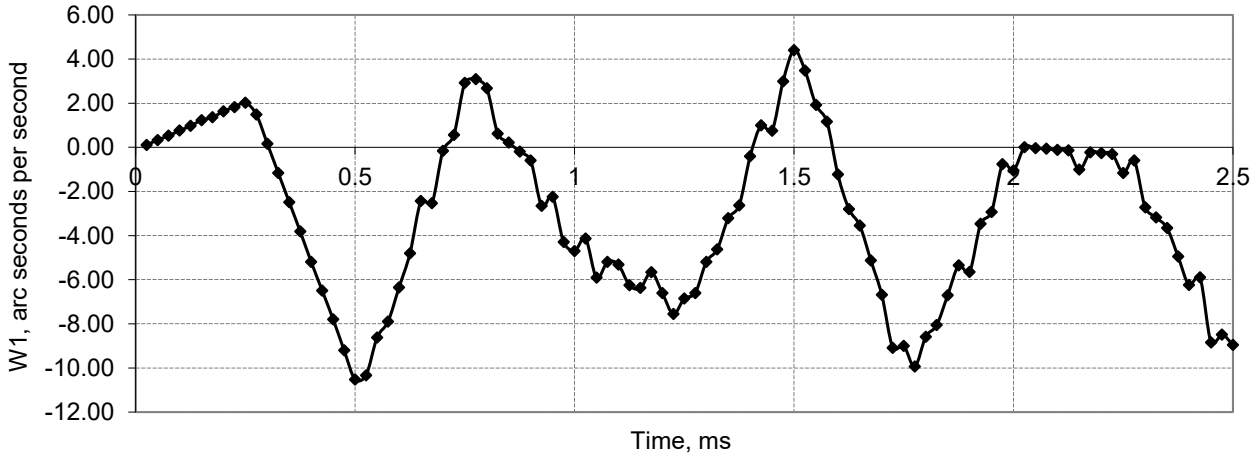

Fig. 17. Projection of angular velocity onto the $X_{\{E\}}$ axis of the instrument coordinate system

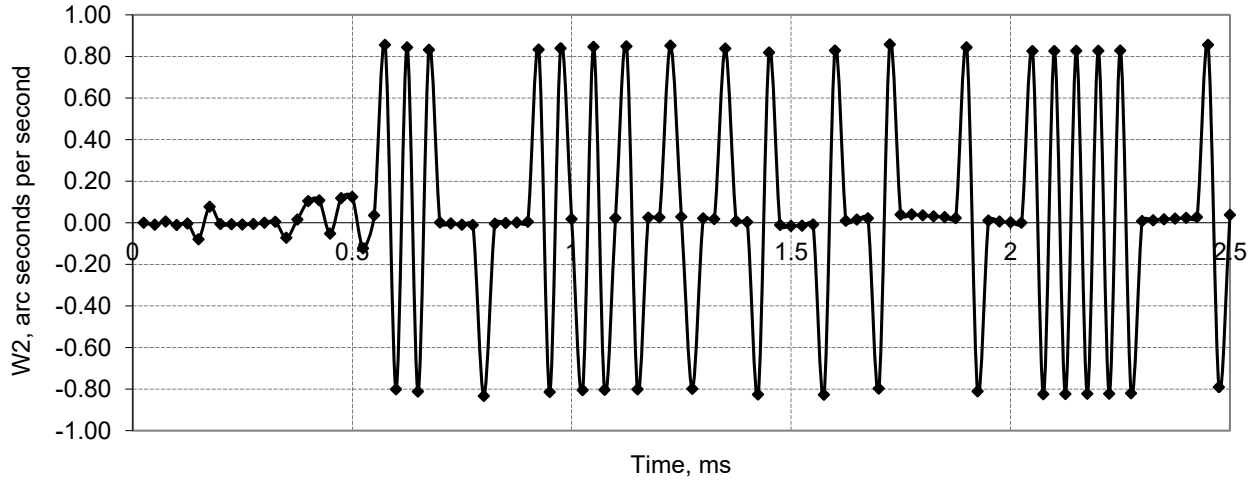

Fig. 18. Projection of angular velocity onto the $Y_{\{E\}}$ axis of the instrument coordinate system

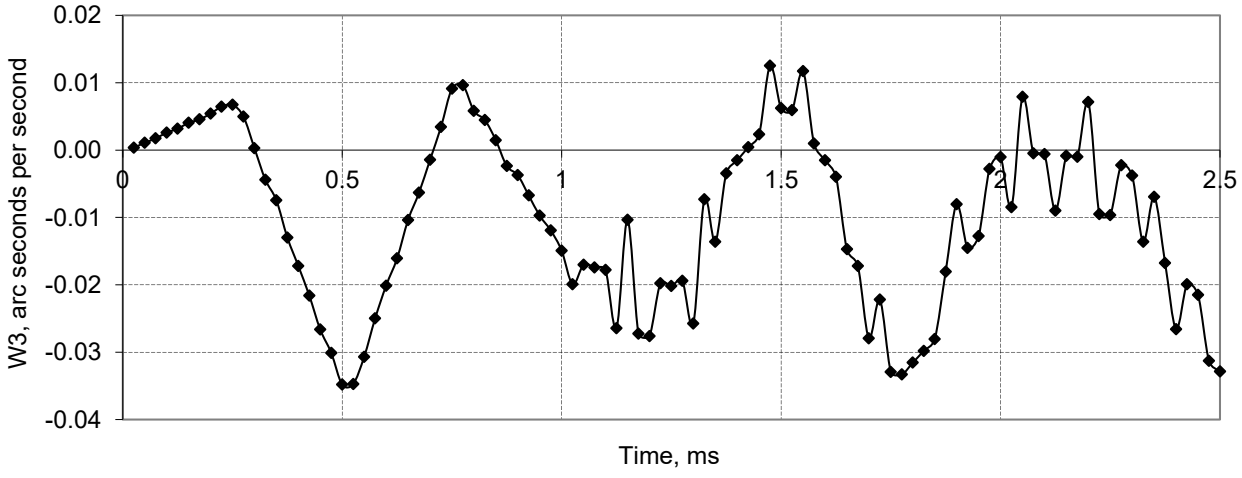

Fig. 19. Projection of angular velocity onto the $Z_{\{E\}}$ axis of the instrument coordinate system

The misalignment parameters are introduced through the following model. Let the axis of sensitivity of the fiber-optic gyroscope (FOG) in the undisturbed state be directed along the $Y_{\{E\}}$ axis of the instrument coordinate system (Fig. 16). The FOG is fixed in a cubic element (Fig. 20), which corresponds to the spacecraft orientation determination unit, at three points *A*, *B*, *C* (Fig. 12), which in the undisturbed state are located in a plane perpendicular to the $Y_{\{E\}}$ axis. These points create a triangle.

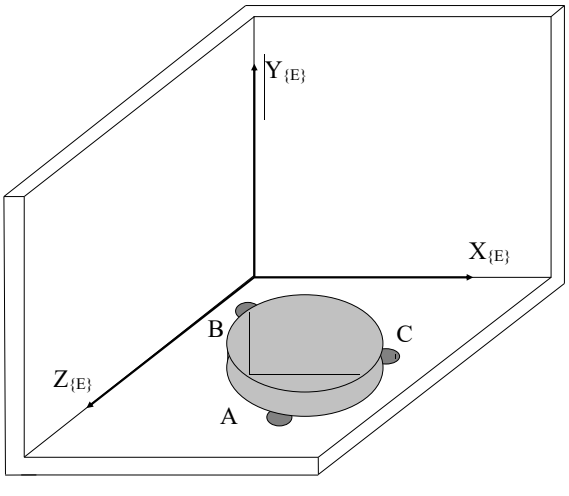

Fig. 20. Mounting a fiber optic gyroscope in a cubic element

During the simulation of thermal deformation of a cubic element for one hour when heated from –10 °C to +40 °C, the displacement values of each of the points *A*, *B*, *C* relative to PCS were obtained (Fig. 13–15). The heating continued at an almost constant velocity. With the specified temperature varying, the modulus of the vector of motion of the points relative to the initial state increased to 2.5 mm. The actual direction of the sensitivity axis was determined from the following formula:

$$\overline{n} = \frac{\overline{r}_{BA} \times \overline{r}_{BC}}{||\overline{r}_{BA} \times \overline{r}_{BC}||}, \quad (11)$$

where $\overline{n}$ is the unit vector coinciding with the sensitivity axis; vectors $\overline{r}_{BA} = \overline{r}_{BA}^{(0)} + \Delta\overline{r}_B - \Delta\overline{r}_A$, $\overline{r}_{BC} = \overline{r}_{BC}^{(0)} + \Delta\overline{r}_B - \Delta\overline{r}_C$ are calculated from $\overline{r}_{BA}^{(0)}$, $\overline{r}_{BC}^{(0)}$ – known design (nominal) values of vectors connecting points *A* and *C* with point *B*; $\Delta\overline{r}_A$, $\Delta\overline{r}_B$, $\Delta\overline{r}_C$ – displacements of the corresponding points determined through thermal deformation modeling. All vector quantities are specified in the inertial coordinate system (CS), which at the initial moment of time coincides with the instrument coordinate system. When the engine is turned on, the instrument CS participates in oscillations.

The misalignment parameter of the actual direction of the sensitivity axis compared to the undisturbed (nominal) direction coinciding with the $Y_{\{E\}}$ axis is defined as:

$$\propto = \arcsin\left(\sqrt{n_1^2 + n_3^2}\right), \quad (12)$$

where n_1, n_3 are the first and third components of vector $\overline{n}$. Taking into account the modeling results for the misalignment parameter (12), the dependence on the FOG temperature was obtained, shown in Fig. 21. The dependence of the projections of the unit sensitivity axis on the *X*, *Z* axes is shown in Fig. 22. The nominal position of the sensitivity axis corresponds to the zero values of the projections.

The total deviation of the axis from the nominal direction is about 150 arcseconds.

Using the angular velocity shown in Fig. 17–19 and the misalignment parameter depicted in Fig. 21, the measurement error of FOG directed along the *Y* axis is determined from the following formula:

$$\Delta\omega = (\overline{n}, \overline{\omega}) - \omega_2, \quad (13)$$

where $\overline{n} = (n_1, n_2, n_3)$ – unit vector from (11), directed along OC; $\overline{\omega} = (\omega_1, \omega_2, \omega_3)$ – angular velocity vector from (10) in projections on the axis of the instrument SC; ω_2 is the second component of the velocity vector, which is the reference value of FOG measurement under consideration.

The dependence of the magnitude of FOG error, which occurs at 100 points of measurements of the instantaneous angular velocity during 2.5 ms of high-frequency oscillations, is shown in Fig. 23.

In Fig. 23, the following notations are used: the markers rhombus, square, triangle, and dot correspond to the values of the misalignment parameter of 30, 60, 110, and 150 arc seconds, respectively. The indicated misalignment values, in turn, correspond to the FOG temperature of –3 °C, +7 °C, +25 °C, and +38 °C. The plots shown demonstrate the influence of different temperatures on the measurement error of a fiber-optic gyroscope due to its misalignment parameter under conditions of high-frequency oscillations.

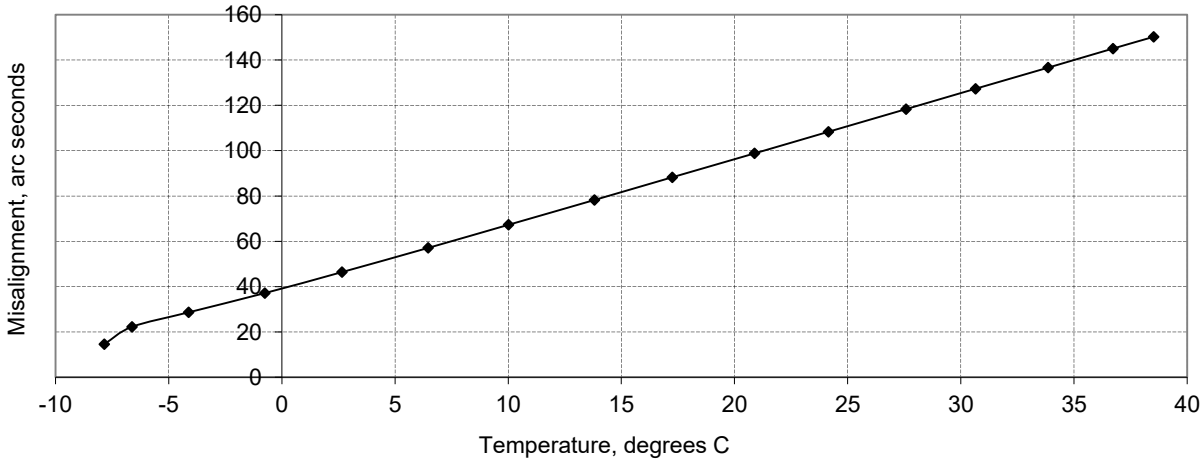

Fig. 21. Dependence of the misalignment parameter on the temperature of a fiber-optic gyroscope

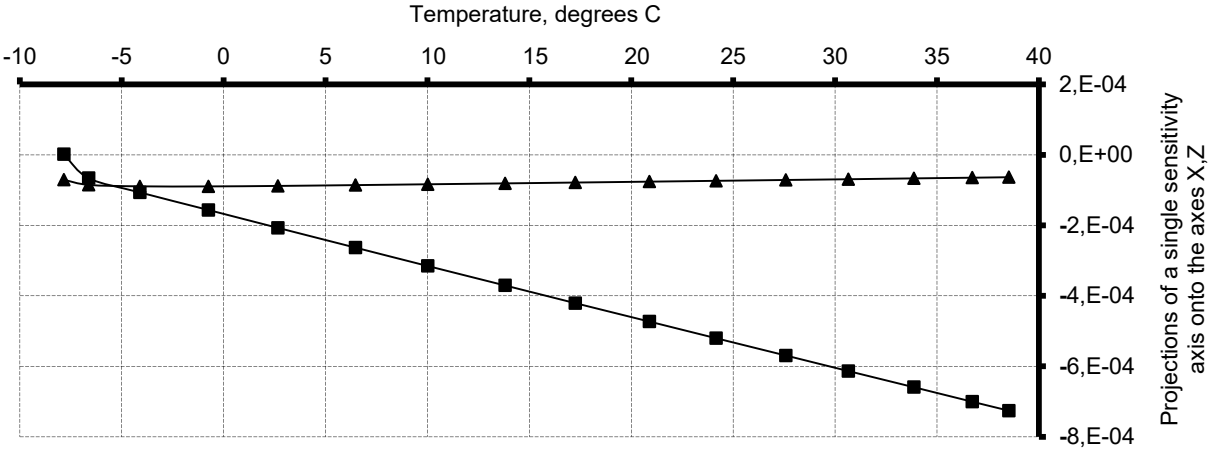

Fig. 22. Dependence of the projections of the sensitivity axis on the *X* (square marker) and *Z* (triangular marker) coordinate axes on the temperature of a fiber-optic gyroscope

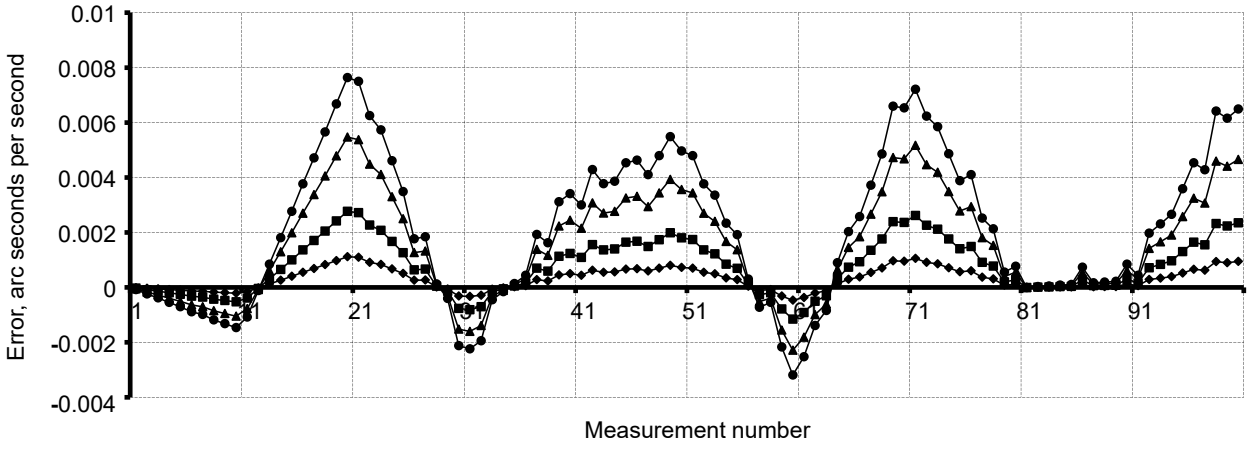

Fig. 23. Measurement error of a fiber-optic gyroscope in dynamics for different values of the misalignment parameter

6. Discussion of results based on determining the influence of thermomechanical loads on the measurement errors of a fiber-optic gyroscope

Our results of modeling thermomechanical deformation of spacecraft structural elements indicate the possibility of using the method of joint analysis of the thermal and stress-strain state to determine the deformation of models of instruments located on spacecraft. In the course of this study, a method for assessing the deformed state of structural elements and instruments under the action of vibration and temperature influences was proposed and implemented. Thanks to the use of the numerical approach chosen for this purpose, based on the application of FEM, numerical results were obtained in the form of distributions by model values of stresses and displacements. Studies on the reliability of

solutions, based on determining the convergence of numerical results when using finite element models with different numbers of elements, allowed us to rely on the obtained time dependences of the displacements of instrument's points for further determining the influence of the considered thermomechanical loads on the measurement errors of fiber-optic gyroscopes.

The above distributions and plots of node displacements when analyzing rocket vibrations at launch (Fig. 2, 3, 5, 6) demonstrate that the total displacements are small and do not exceed $0.77 \cdot 10^{-2}$ mm. According to the results of numerical modeling, it was determined that during the vibrational motion of the nodes, it is possible to distinguish motion mainly in the plane (the third component is practically zero). For example, at node C, the order of the magnitude of components u and v is 10^{-6} m, and w – 10^{-11}. It was determined (Fig. 7) that the maximum stresses are realized at the points of the combustion chamber, and on the instrument, they are small and do not exceed 2.2 MPa, which is permissible during operation.

The temperature distributions determined by solving the unsteady heat conduction problem (Fig. 10) are characterized by significant heterogeneity in the model volume and in time, therefore their consideration in the further analysis of the deformed state is necessary. The time dependences of displacements (Fig. 13–15) show that in the presence of thermal strains arising due to the permanent varying in the temperature field, a significant change in the displacements occurs. In this case, the values of the components of displacement vector u (in the direction of the coordinate axis x) are significantly larger than in the other two directions.

Taking into account the displacements of base points of the structure during vibration and thermal deformation at the points of attachment of FOG, specific indicators of the influence of thermal fields on the misalignment parameter of the fiber-optic gyroscope as part of the onboard control system of the spacecraft were obtained.

The unevenness of the displacements of points of the structure (Fig. 4, 5), which occurs during the operation of the jet engine, generates a rotational motion of the studied part of the structure with an angular velocity of small amplitude, but significant frequency (Fig. 17–19). This angular velocity is measured by a gyroscope to calculate the current orientation of the spacecraft. The main factor in the error of such measurements is the non-stationary nature of the temperature, which, due to thermal deformation at the points of attachment of FOG to the body (Fig. 13–15), leads to a discrepancy between the actual direction of the FOG sensitivity axis (Fig. 22) and the nominal direction. Such a discrepancy is characterized by the misalignment parameter, for which a significant dependence on temperature has been established (Fig. 21). The presence of such misalignment when measuring angular velocity (Fig. 17–19) is accompanied by a measurement error (Fig. 23), which will increase up to 8 times for different temperature values.

Thus, the theoretical result of our study is the revealed significant dependence of the FOG misalignment parameter and, accordingly, the measurement error on temperature. From a practical point of view, such a dependence means that to achieve high-precision orientation, it is necessary to reduce the influence of thermal deformation of the structure on FOG. This is possible either by rationally choosing the location of FOG on board the spacecraft, where there are no large temperature gradients, or by introducing algorithmic compensation of the measurement error into the mathematical support to the spacecraft control system.

The advantage of the devised procedure for modeling thermomechanical deformation and calculating the error in gyroscope measurements due to the influence of the misalignment parameter is that the modeling is carried out under typical temperature conditions inherent in the orbital flight of the spacecraft, and under specific characteristics of the vehicle's motion. But the procedure is, at the same time, universal and could be easily adapted for any thermomechanical loads.

A limitation of our study is that the task to determine the influence has been considered for one gyroscope. To assess the accuracy in determining the orientation of the spacecraft by the onboard system, it is necessary in the future to apply the devised mathematical modeling procedure for three FOGs with mutually orthogonal sensitivity axes.

7. Conclusions

1. The results of a joint analysis of the stress-strain state of structural elements of rocket and space technology instruments have been obtained. It includes modeling the stress-strain state of the object using the finite element method and determining the current displacements of the gyroscope attachment points due to thermomechanical loading. It has been established that in the presence of thermal strains arising from the permanent varying of the temperature field, significant displacements of attachment points of up to 2.5 mm occur.

2. The basic formula dependences for determining the measurement error of a fiber-optic gyroscope (FOG) were obtained. By numerical modeling of the deformed state under the above conditions, the influence of temperature changes on the measurement error of FOG was analyzed. An auxiliary result is the formulas for determining the reference angular velocity of the instrument coordinate system at a given location on board the spacecraft under conditions of high-frequency oscillations. The time dependences for different temperature conditions of FOG measurement errors caused by the gyroscope misalignment were obtained. For the given modeling conditions, it was established that when the FOG temperature changes by 40 °C, the measurement error caused by the misalignment would increase 8 times. In this case, the misalignment itself would reach hundreds of arc seconds. This is an unacceptably large value that could lead to low control accuracy. Therefore, for the effective use of FOG, compensation of the temperature effect is required using any of the known methods. At the same time, the initial data for such methods can be obtained using the devised procedure for determining the influence of thermal strains on the errors of FOG measurements.

Conflicts of interest

The authors declare that they have no conflicts of interest in relation to the current study, including financial, personal, authorship, or any other, that could affect the study, as well as the results reported in this paper.

Funding

This work was supported by the EURIZON project, which is funded by the European Union under grant agreement No. 3053.

Data availability

The data will be provided upon reasonable request.

Use of artificial intelligence

The authors confirm that they did not use artificial intelligence technologies when creating the current work.

Acknowledgments

The authors express their gratitude to the EURIZON project, funded by the European Union, for supporting the research.

References

1. Nurgizat, Y., Balbayev, G., Galayko, D. (2021). Solar sensor for Cubesat attitude determination. 2021 28th IEEE International Conference on Electronics, Circuits, and Systems (ICECS), 1–5. https://doi.org/10.1109/icecs53924.2021.9665513
2. Zbrutsky, O., Meleshko, V., Ganja, A., Tarnavsky, S., Bondarenko, O., Pjnomarenko, S., Saurova, K. (2022). System definition of micro - nano satellite orientation. MECHANICS OF GYROSCOPIC SYSTEMS, 43, 46–60. https://doi.org/10.20535/0203-3771432022275282
3. El-Sheimy, N., Youssef, A. (2020). Inertial sensors technologies for navigation applications: state of the art and future trends. Satellite Navigation, 1 (1). https://doi.org/10.1186/s43020-019-0001-5
4. Wang, X., Cui, Y., Cao, H. (2023). Temperature Drift Compensation of Fiber Optic Gyroscopes Based on an Improved Method. Micromachines, 14 (9), 1712. https://doi.org/10.3390/mi14091712
5. Kucherenko, O. (2024). Methods of reducing the influence of temperature gradients on the sensitivity of fiber-optic gyroscope. Bulletin of Kyiv Polytechnic Institute. Series Instrument Making, 67 (1), 13–17. https://doi.org/10.20535/1970.67(1).2024.306720
6. Ban, J., Chen, G., Meng, Y., Shu, J. (2022). Calibration method for misalignment angles of a fiber optic gyroscope in single-axis rotational inertial navigation systems. Optics Express, 30 (5), 6487. https://doi.org/10.1364/oe.449629
7. Gorev, V., Pelemeshko, A., Zadorozhny, A., Sidorchuk, A. (2018). Thermal deformation of 3U CubeSat in low Earth orbit. MATEC Web of Conferences, 158, 01013. https://doi.org/10.1051/matecconf/201815801013
8. Bonnici, M., Mollicone, P., Fenech, M., Azzopardi, M. A. (2019). Analytical and numerical models for thermal related design of a new pico-satellite. Applied Thermal Engineering, 159, 113908. https://doi.org/10.1016/j.applthermaleng.2019.113908
9. Abdelal, G. F., Abuelfoutouh, N., Gad, A. H. (2013). Finite Element Analysis for Satellite Structures. Springer London. https://doi.org/10.1007/978-1-4471-4637-7
10. Breslavsky, D., Uspensky, V., Kozlyuk, A., Paschenko, S., Tatarinova, O., Kuznyetsov, Y. (2017). Estimation of heat field and temperature models of errors in fiber-optic gyroscopes used in aerospace systems. Eastern-European Journal of Enterprise Technologies, 1 (9 (85)), 44–53. https://doi.org/10.15587/1729-4061.2017.93320
11. Reza Eslami, M., Hetnarski, R. B., Ignaczak, J., Noda, N., Sumi, N., Tanigawa, Y. (2013). Theory of Elasticity and Thermal Stresses. In Solid Mechanics and Its Applications. Springer Netherlands. https://doi.org/10.1007/978-94-007-6356-2
12. Parkus, H. (1976). Thermoelasticity. Springer Vienna. https://doi.org/10.1007/978-3-7091-8447-9
13. Nowacki, W. (1986). Thermoelasticity. Oxford, 578.
14. Day, W. A. (1985). Heat Conduction Within Linear Thermoelasticity. In Springer Tracts in Natural Philosophy. Springer New York. https://doi.org/10.1007/978-1-4613-9555-3
15. Zienkiewicz, O. C., Taylor, R. L., Fox, D. D. (2014). The finite element method for solid and structural mechanics. Elsevier. https://doi.org/10.1016/c2009-0-26332-x
16. Stolarski, T. (2018). Engineering analysis with ANSYS software. Butterworth-Heinemann. https://doi.org/10.1016/c2016-0-01966-6
17. Breslavsky, D., Morachkovsky, O., Tatarinova, O. (2014). Creep and damage in shells of revolution under cyclic loading and heating. International Journal of Non-Linear Mechanics, 66, 87–95. https://doi.org/10.1016/j.ijnonlinmec.2014.02.005
18. Breslavskii, D. V., Metelev, V. A., Morachkovskii, O. K. (2015). Anisotropic Creep and Damage in Structural Elements Under Cyclic Loading. Strength of Materials, 47 (2), 235–241. https://doi.org/10.1007/s11223-015-9653-z
19. Breslavsky, D. V., Morachkovsky, O. K., Tatarinova, O. A. (2008). High-temperature creep and long-term strength of structural elements under cyclic loading. Strength of Materials, 40 (5), 531–537. https://doi.org/10.1007/s11223-008-9067-2
20. Uspenskyi, V. B., Kuznyetsov, Y. O., Shyriaieva, N. V. (2021). The Location Optimization of the On-Board Measuring System for Moving Objects Accounting Vibration. 2021 IEEE 2nd KhPI Week on Advanced Technology (KhPIWeek), 317–322. https://doi.org/10.1109/khpiweek53812.2021.9570091